Title	Defocus-corrected analysis of the foveal Stiles-Crawford effect of the first kind across the visible spectrum
Authors(s)	Lochocki, Benjamin, Vohnsen, Brian
Publication date	2013-10-18
Publication information	Lochocki, Benjamin, and Brian Vohnsen. “Defocus-Corrected Analysis of the Foveal Stiles-Crawford Effect of the First Kind across the Visible Spectrum.” IOP Publishing, October 18, 2013. https://doi.org/10.1088/2040-8978/15/12/125301.
Publisher	IOP Publishing
Item record/more information	http://hdl.handle.net/10197/13058
Publisher's version (DOI)	10.1088/2040-8978/15/12/125301

Benjamin Lochocki and Brian Vohnsen 2013 J. Opt. **15** 125301, is available online at DOI: https://doi.org/10.1088/2040-8978/15/12/125301

*Defocus-corrected analysis of the foveal Stiles-Crawford effect of the first kind across the visible spectrum

Benjamin Lochocki* and Brian Vohnsen
Advanced Optical Imaging Group, School of Physics, University College Dublin, Dublin 4, Ireland

*E-mail: benjamin.lochocki@ucdconnect.ie

Abstract
The Stiles-Crawford effect of the first kind describes a gradually-diminished visibility of light that enters the eye towards the pupil rim. Although of retinal origin, it is commonly described by a Gaussian pupil apodization whose width is determined by a directionality parameter that depends on retinal eccentricity, wavelength and spatial coherence of the light. As the measurements are done psychophysically they are prone to subjective variations and difficult to obtain across the visible spectrum. In this work, requirements for accurate refractive correction when determining the directionality parameter at any given wavelength are discussed and we show that a current-controlled tuneable liquid-polymer lens provides a convenient means to accomplish this without requiring mechanical readjustments. This may be the most convenient way to combat defocus across the visible spectrum in the analysis of the Stiles-Crawford effect as demonstrated through experiments and with a detailed Zemax eye-and-system analysis. The results obtained are discussed in relation to myopia and a reduced directionality for highly myopic eyes.

Keywords: Stiles-Crawford effect, cone photoreceptors, chromatic aberrations, human eye, waveguiding, myopia

1. Introduction

The Stiles-Crawford effect of the first kind (SCE) manifests a reduced luminous efficiency of obliquely incident light on the retina that originate in the light-to-photoreceptor coupling [1,2]. This visibility reduction becomes significant at large pupil diameters where the efficiency for rays entering the eye near to the pupil rim may typically be only about a quarter of its maximum value close to the pupil centre. Although studied psychophysically for humans, it is also understood to be present in other vertebrates due to the similarity of their retinal receptors and the observation of single-cone waveguide modes in retinal tissues from different species [3]. Related objective methods have shown directional sensitivity of the retina using electroretinograms such as in recently-reported macaque monkey studies [4]. The biological raison d'etre that underpins the directional effect is believed to relate to a reduced sensitivity to intraocular light scattering and aberrations [5] and to economization of visual pigments by light concentration [6]. Although the retinal origin of the SCE has been known for 80 years its underlying optical mechanisms remain somewhat unclear due to the difficulties in obtaining accurate directional visibility measurements and a number of mechanisms that include cellular waveguiding, photopigment absorption, scattering, bleaching and self-screening that individually, or in conjunction, play important roles towards establishing a completely satisfactory understanding of the effect and its consequences [7].

The SCE is analyzed by translating a narrow test source in a Maxwellian view across the pupil while monitoring subjective changes in visibility of the resulting test field in comparison to that of an adjacent or overlapping reference field produced by light entering the eye near to the pupil centre. Tiny secondary sources are used both for the reference and for the test lights as this minimizes the impact of monochromatic aberrations and effectively limits the entrance to a single pupil point at a time [8]. The relative visibility, η, is commonly expressed by a Gaussian function as a function of the test light pupil entrance point, r, and a characteristic directionality parameter, ρ, that relates to the inverse width of the function (a large value implies a more narrow visibility tuning angle) with a typical value of 0.05/mm^2 for the foveal region.

A review of the literature reveals a large spread in foveal directionality parameters for different subjects, methods and wavelengths used. One approach uses a bipartite field [1,9-15] in which the subject adjusts the brightness of a test field until a satisfactory match has been obtained to that of an adjacent reference field. Another approach makes use of flickering overlapping fields adjusted in brightness until a visibility difference is no longer perceivable [1,11,16-20]. Early studies used white light [1,9] but most later studies have used narrowband light in the yellow to red spectral range. Stiles reported values for ρ from 0.053/mm^2 to 0.072/mm^2 in the range from λ = 440 nm to 720 nm [9], Alpern and Kitahara reported a strong drop in directionality in the deep-blue range as low as 0.00072/mm^2 (400.2 nm) but raised to 0.0692/mm^2 if numerically corrected for absorption by the crystalline lens [16], Rativa and Vohnsen found a reduced directionality in the deep-blue range [15], in the green (552 nm) Enoch reported 0.045/mm^2 [11], Singh *et al*. reported higher values in a study of accommodation in relation to the SCE using orange light (620 nm) with 0.145/mm^2 (horizontal) and 0.106/mm^2 (vertical) [17], also in the orange (621 nm) Nordby and Sharpe found 0.054/mm^2 [18], Enoch and Hope in the orange-red 0.053/mm^2 to 0.058/mm^2 [19], Kruger *et al.* reported in the red (633 nm) 0.052/mm^2 [12], and Applegate and Lakshminarayanan in the red (670 nm) 0.047/mm^2 (horizontal) and 0.053/mm^2 (vertical) [20]. A full spectral analysis of the directionality parameter for individual subjects has to our knowledge only been reported by Stiles [9], Enoch and Stiles [10], Alpern and Kitahara [16] and most recently by our group [14]. Such analysis is required to give insight into the surprisingly narrow acceptance lope of the cone photoreceptors whether acting as waveguides or as an ordered array of visual pigments [7]. It has been suggested that longitudinal chromatic aberrations of the eye may play a role for accommodation [12,21] and that defocus can impact the determination of the directionality parameter. Indeed, a slight reduction in directionality has been found for highly myopes using orange light (620 nm longpass filter) [13]. Singh *et al.* reported an increased directionality of ~3% per dioptre of increased accommodation stimulus although this may also have been influenced by artefacts related to higher-order aberrations and accommodative lag [17].

Analysis with Maxwellian view and paralyzed accommodation is obviously different from that of a normal viewing situation through the natural pupil where the eye may accommodate and an integrated Stiles-Crawford function is at work [22]. Nevertheless, it is considered to represent accurately the full pupil response for perfectly incoherent light [1,11,23]. In previous analyses of the SCE, refractive errors have been corrected with lenses [20] and with an optical trombone [17]. At different wavelengths the individualized refractive correction needs to be altered which has been realized by axially translating the limiting aperture of the incident light [16]. This becomes challenging when scanning the test source across the pupil as chromatic defocus may cause a retinal shift of the viewed test field. Stiles and Crawford [1,9] compensated for this by readjusting the transverse location of the aperture for the traversing beam at each pupil entrance point. Enoch [13,19] and others have used a large background stimulus in flickering experiments to reduce this complication while still requiring re-centring for each scan position to minimize variations. This is feasible at one wavelength but problematic across a spectral range as any retinal translation of the viewed field, even if minor, is a result of uncorrected refractive error. Axial chromatic error of the eye may be strongly reduced with a Bedford and Wyszecki-type lens [24], but an attractive alternative is a completely automated system that can compensate both this unwanted shift of the traversing test field and the subjective refractive correction while also correct remnant errors of the system at any given wavelength.

The purpose of this study is to examine the feasibility of an automated SCE characterization system using a current-driven tuneable liquid polymer lens (i.e. tuneable focus) for defocus correction at any test wavelength. The large spread in reported directionality parameters and the very limited insight into its spectral dependence makes it pertinent to explore novel techniques that eventually may pave the way for a complete understanding of the SCE under a variety of conditions that elucidate its role in vision for both healthy eyes and in eyes with pathologies. The tuneable focus lens is build into a computer-controlled SCE characterization system with liquid-crystal tuneable wavelength and liquid-crystal intensity controls that are all adjusted by the subject via a handheld game console. This system permits SCE characterisation across the visible spectrum providing directionality parameters that are in good agreement with most other reported values listed above and are more accurate than our previous data for the same subjects obtained without chromatic defocus correction [14].

This paper is organized as follows: in Section 2 the experimental setup and measurement procedure is described, in Section 3 the system and the impact of the tuneable focus lens is analyzed, Section 4 contains the experimental results and the discussion that includes the role that myopia may play for accurate SCE analysis, and in Section 5 we present the conclusions.

2. Experimental setup and method for Stiles-Crawford characterization

The devised system and the experimental procedure followed are described in the following.

2.1 Experimental setup

A bipartite field system has been constructed that improves on our former setup used in the analysis of the Stiles-Crawford effects of the first and second kind [20]. The setup is shown schematically in Fig. 1. A fibre-guided ∅1.6 mm tungsten-halogen source is projected, using a set of achromatic lenses for both the reference and test beams, to form two secondary sources with a diameter of 0.2 mm in the pupil plane for Maxwellian view. A tuneable liquid-crystal filter (Meadowlark, TOF-SB-VIS) is used for wavelength and bandwidth control across the visible spectrum while a tuneable liquid-crystal attenuator (Meadowlark, LVA-100-λ) is used for brightness control of the test beam. A mirror is used to split the incident light into two parts that are recombined again at the scanning mirror whereby the scanning mirror itself blocks half of the reference beam. Horizontal pupil scans were realized using a galvanometric scanning unit (General Scanning VM500+). The resulting retinal image is a juxtaposition of two half-circles constituting the bipartite field with a viewing angle of approximately 1.5 visual degrees set by two 5.0 mm circular apertures mounted near the scanning mirror. The bipartite fields appear completely uniform in brightness and in colour to the viewer as all light is propagating paraxially within the angular limits of the tuneable filters used (< 6°). The intensity of the light source is adjusted to appear equally bright in photopic conditions to the subject across the visible spectrum to avoid the drop-off in the blue spectral range of the light source and to avoid bleaching near the peak of sensitivity of the human eye. For green light (at 550 nm central wavelength) the combined power of the reference and test light is approximately 3 nW at the pupil when both enter the eye at the point of maximum visibility. It is well established that the foveal SCE is insensitive to the actual field brightness used (whereas for the parafovea a transition exists from only weakly directional scotopic to highly directional photopic conditions) [25]. For oblique incidence also a minor hue shift (the Stiles-Crawford effect of the second kind) is present within the bandwidth of the quasi-monochromatic light used that can complicate a satisfactory brightness match of the bipartite field [9,14]. Wavelength detuning or adjustable trichromatic illumination can improve the colour match that for simplicity will not be considered further here.

When the entrance point is changed by the scan mirror (a mechanical scan range of 1.1° produces a complete sweep across an 8 mm pupil) small differences in optical path are introduced. Clockwise rotation of the mirror slightly increases the path between the f500 and f200 lenses whereas for counter-clockwise rotation it is slightly decreased as the scanner axis is located centrally below the mirror. This causes small axial variations and wavefront tilt in the test beam near the eye. A further complication when changing the wavelength is the fact that the focal length of each achromatic doublet lens varies slightly on the order of 0.2% across the visible spectrum (increasing at long wavelengths). These minor variations need correction in addition to the ocular aberrations of the subject for each position of the scanner and for each chosen wavelength. To combat these, a tuneable defocus correction has been implemented with a current-controlled tuneable positive lens (Optotune EL-10-30 LD, f_1 = 45 to 120 mm) in combination with a negative achromatic lens (f_2 = -75 mm) placed directly in front of the eye. Together, these lenses allow the refractive power to be adjusted smoothly in the range of approximately -4 to +12 dioptres. When compared to mechanical solutions with shifting apertures, changing corrective lenses, or adjusting an optical trombone, the tuneable focus lens has the advantage of allowing faster electronically-adjusted refractive correction of individual subjects for each pupil point and at each wavelength setting.

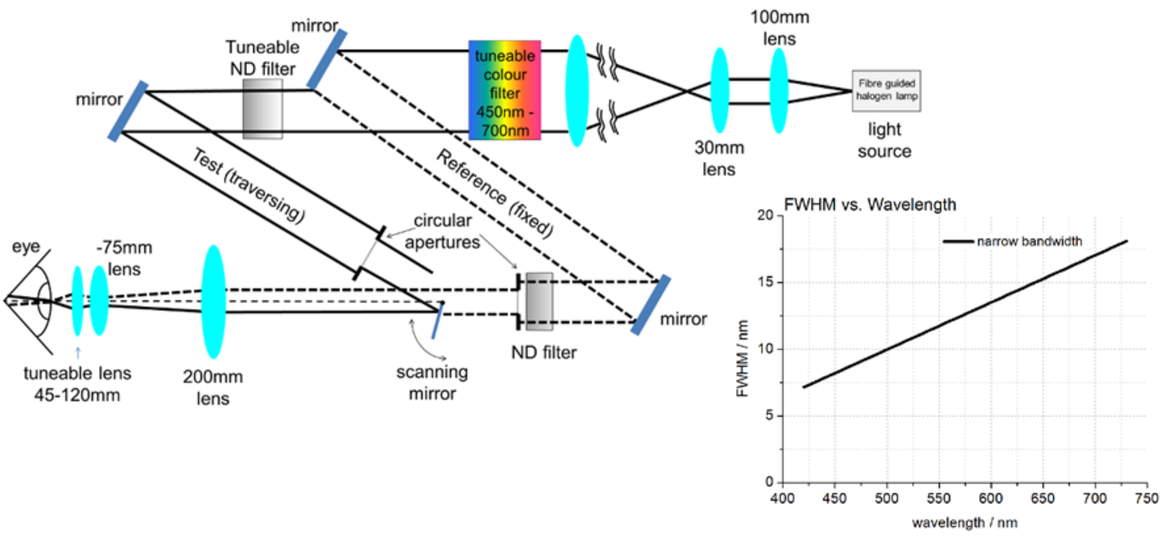

Figure 1. Left: Schematic of the bipartite setup used in the analysis of the SCE with dual Maxwellian view. Two mirrors are used to project the reference field from the fibre-guided source to the eye pupil and two other mirrors, one of which is the scanning mirror, is used to project the traversing test beam from the fibre source onto the pupil. The scanning mirror is also used to block half of the reference beam thereby creating the bipartite field. All lenses are AR-coated achromatic doublets with the exception of the current-controlled tuneable plano-convex lens mounted in front of the eye at a distance of approximately 14 mm (vertex distance). **Lower right:** Narrow bandwidth characterization (FWHM: full width at half maximum) of the tuneable liquid-crystal colour filter showing a linear increase across the visible spectrum.

Prior to SCE characterisation, the system has been accurately calibrated in the entrance pupil plane (position calibration using a CCD camera), in the retinal plane using an artificial eye (f25 achromatic lens) and a CCD camera to validate the bipartite field quality, and a precision optical power meter to determine the incident power of the reference and test light, respectively. The tuneable attenuator (ND filter) has been calibrated in terms of light power reaching the pupil plane as required for a proper determination of relative visibility. The entire system is computer-controlled via LabView (National Instruments) that also analyzes the data for best fitting functions and directionality parameters. The numerical fitting procedures, based on nonlinear Levenberg-Marquardt algorithm for chi-square minimization, have been cross-checked and found in correspondence with those of OriginPro 8.6 (OriginLab) in terms of R-squared values.

2.2 Experimental procedure

One eye of each author has been analyzed in this study: BL (33 years, left eye) and BV (43 years, right eye) both with normal emmetropic vision. Procedures were approved by the Human Research Ethics Committee at University College Dublin. Pupils were dilated and accommodation partially paralyzed using 2 drops of 1% tropicamide repeated every two hours to maintain pupil dilation throughout the duration of the experiment. A bite bar was used to minimize unwanted head and eye motion. The entrance point of the traversing test light was varied across the full pupil while adjusting the X-Y-Z position of the bite bar to ensure proper alignment of each subject at the point of maximum visibility prior to any measurements. The subject gazed at all times on the sharp 5 mm vertical edge of the galvanometric-mounted scanning mirror in the middle of the bipartite field.

Measurements were made across the visible spectrum from 450 to 700 nm at eleven distinct wavelengths with the tuneable colour filter set for narrowband operation of approximately 10 nm width (but increasing with wavelength as shown in Fig. 1) [14]. Prior to SCE characterisation, the tuneable focus lens was first used to correct chromatic defocus error for each subject (including the minor chromatic changes inherent in the system) across the visible spectrum to obtain an individualized calibration curve for the correction. Without this correction, the juxtaposed test and reference in the bipartite retinal field would wander about for different pupil entrance points and for different wavelengths. Thus, at each set wavelength the entrance point was varied from side-to-side of the pupil while the subject adjusted the tuneable focus lens to minimize unwanted translation of the test light in the bipartite field coinciding with the setting of sharpest focus of the scanning mirror edge. The resulting current-versus-wavelength data fitted to a linear dependence are shown in Fig. 2 for the two subjects. Converted into focal length this corresponds to a range of 70-85 mm for subject BL and 77-91 mm for subject BV based on the manufacturer's data. This range corresponds to the approximately 2 dioptre focal difference of the eye from the blue to the red end of the spectrum. The difference between the two subjects reveals a distinct refractive state of their unaccommodated eye that corresponds to an approximately 8 mm difference in the tuneable focus lens setting. The spacing between the eye and lens assembly might be slightly different for the two subjects but it is also suggestive of a slight difference in axial length of the two subject eyes. An estimate based on the effective refractive power based on Fig. 2 suggests that the axial length of subject BL's eye is approximately 0.7 mm longer than that of subject BV. To examine if this is the case, the axial length of both subject eyes was measured using two commercial instruments: (i) Allegro Biograph (WaveLight) and (ii) IOLMaster (Carl Zeiss Meditec). Both techniques gave similar results with subject BV's axial eye length between (i) 23.27 mm (ii) and 23.29 mm and subject BL's axial eye length between (i) 25.01 mm and (ii) 25.08 mm. Thus, although in the right direction, in this case the value based on Fig. 2 alone underestimates the actual difference between the subjects. The clinical measurements also produced values for refractive error on a ∅6.50 mm pupil that for subject BV was

0.09D sphere and -0.65D cylinder (spherical equivalent of -0.24D) and for subject BL was 0.21D sphere and -0.14D cylinder (spherical equivalent of 0.14D).

Each experimental SCE analysis series consists of 4 horizontal across-the-pupil scans and 11 set wavelengths. The starting point for each measurement series is at the initial pupil entrance point of maximum visibility. The pupil entrance point is slightly altered as a function of focal length of the tuneable focus lens but this is compensated for by the scanning mirror positioning calibrated in the plane of the entrance pupil. Thus, for all realized settings, the scanning mirror advanced the entrance point of the projected test source in 14 equal linear steps across the pupil (each step equals 0.5 mm) from x = -3.5 to x = +3.5 mm as confirmed with the CCD camera used for system validation. Thus, the test beam progresses successively from the middle to the right and then to the left of the pupil until a total of 4 traversals have been completed. When this happens the tuneable spectral filter increases the wavelength and the entire procedure is repeated for the new colour. The tuneable focus lens is automatically adjusted to correct the chromatic defocus in accordance with the calibration shown in Fig. 2 beginning in the blue and advancing in steps towards the red end of the spectrum. For each measurement, the subject adjusts the brightness of the test field using the tuneable attenuator to obtain the best possible match with the adjacent reference field (entering the eye at the point of maximum visibility). This adjustment is done by using the computer-controlled gamepad that also triggers the advancement of the scanning mirror in preparation for the next measurement. From this, the relative visibility, η, is calculated as a calibrated power ratio as determined with the optical power meter. Each such visibility comparison and tuning takes typically about 5 to 10 seconds although the subject is free to vary the adaptation time needed before progressing to the next measurement point at the push of a button. Thus, the subject can essentially complete the entire measurement cycle on his own although in all cases the other participant remained present to monitor that everything progressed and that data were stored on the computer correctly.

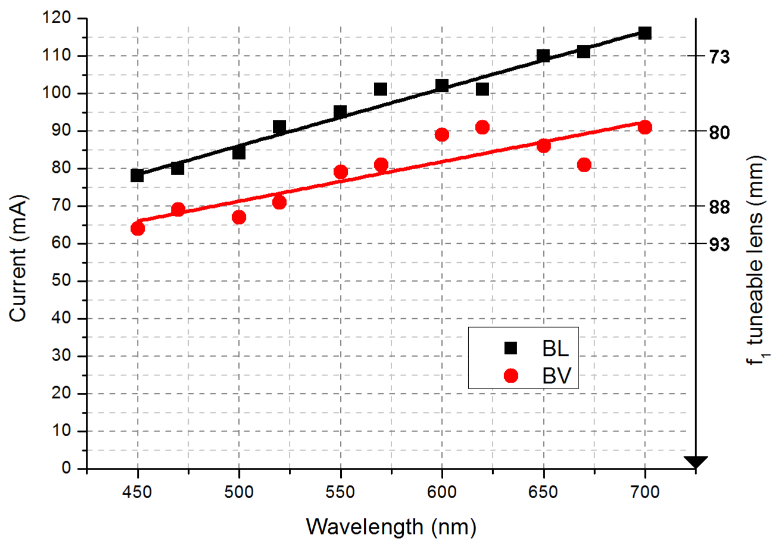

Figure 2. Current-versus-wavelength plots for the tuneable focus lens fitted to linear dependencies for both subjects BL and BV when subjectively correcting for chromatic defocus variations of the eye and (to a lesser degree) system. The current-to-focal length conversion (left and right vertical axes) is based on the manufacturer specifications [26] and indicated here for λ = 525 nm.

3. Model of setup and influence of chromatic defocus

Chromatic aberrations of the eye result in different angles of incidence on the retina across the visible spectrum. The refractive correction needs to be individualized and selected for each set wavelength and pupil entrance point. Fig. 3 shows schematically the impact that refractive and chromatic errors may have if not corrected in the analysis of the SCE. The emmetropic eye may project green light at the ideal retinal location but will need to accommodate or be corrected for the other wavelengths shown (Fig. 3a). The uncorrected myopic case (as well as the hyperopic case) would result in a shift of the rays on the retina away from the tested region (Fig. 3b) and only with proper correction at the wavelength being analyzed, here shown for green, will the light reach the intended retinal location (Fig. 3c).

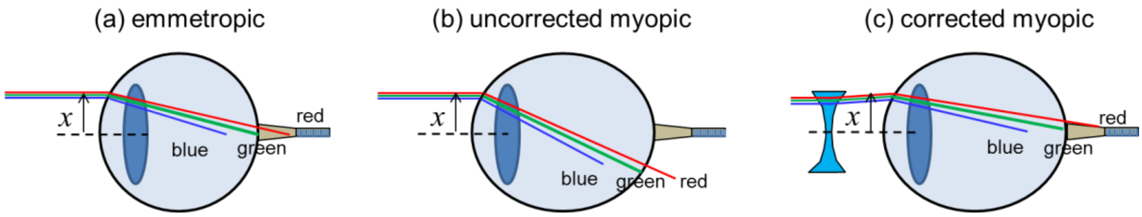

Figure 3. Schematic of the impact of chromatic aberrations for an (a) emmetropic eye where it gives rise to chromatic blur, (b) for an uncorrected myopic eye, and (c) for a corrected (for green light) myopic eye. All are shown for blue, green and red light entering the eye at an off-axis position, *x*. In the ideal cases (a) and (c) the tested wavelength impinges on the correct retinal region reaching the pigments of the photoreceptor cones. In the SCE experiments only one narrowband wavelength is tested at a time being refracted correctly onto the tested region of the retina. For simplicity only one centrally located cone is shown.

3.1 Zemax system and eye model

Corrective lenses and an optical trombone have previously been used to correct for refractive errors of the eye when analyzing the SCE. When changing the wavelength also the axial position of the limiting aperture and its transverse location will need readjustments for each pupil entrance point to avoid relative motion of the bipartite or overlapping flickering fields. Corrections could potentially be done by axially translating the f200 achromatic lens in front of the eye, or with a Badal system, but the range would be limited and it would require mechanical action prior to each measurement. A tuneable focus lens as implemented here offers a rapid and flexible way to correct these refractive errors for each subject across the visible spectrum.

The entire system shown in Fig. 1 has been analyzed using Geometric Image Analysis in the sequential ray-tracing mode of Zemax (Radiant Zemax) using a point source in place of the narrow optical fibre bundle of the source. The chosen eye model is that of Diaz *et al*. [27] with a gradient crystalline lens having age-dependent parameters chosen to equal those of an average 33 year old subject. This eye model includes an approximately 1.6 mm off-axis temporal location of the fovea (positive *x*-axis in the chosen coordinate system). The achromatic lenses correspond to those of the setup (Thorlabs) and have been chosen from the Zemax catalogue. Data for the tuneable focus lens have been provided by the manufacturer [26]. The wavelength was set directly in Zemax rather than via modelling of the tuneable colour filter. A semi-circular aperture was inserted in the traversing beam path and placed in the conjugated plane of the retina to model the test light of the bipartite field. The mirror at the conjugated pupil plane was numerically tilted to simulate scanning across the pupil.

The dispersion of each lens and the eye has been fully implemented in the model as based on the Sellmeier equation.

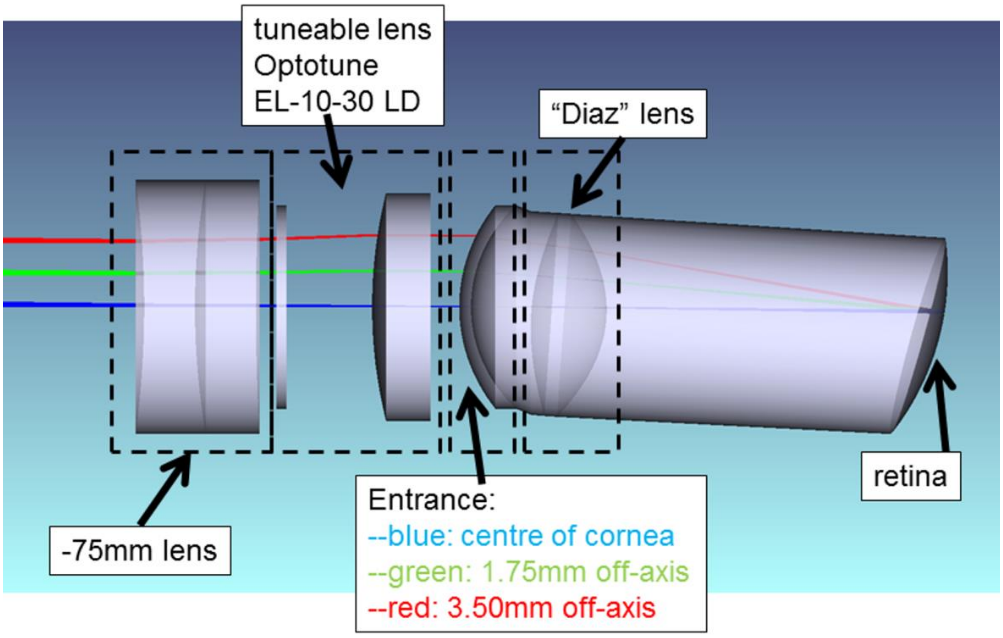

Figure 4. Zoom-in (view from above) on the Zemax model containing the -75 mm achromatic lens, the tuneable focus lens and the eye model with the light being incident from the left. Here, three scan positions of the traversing test beam are shown corresponding to a central location (x = 0, blue), off-axis (x = 1.75 mm, green) and near the pupil rim (x = 3.50 mm, red).

3.2 Zemax analysis of bipartite Stiles-Crawford characterization

The impact of refractive correction for different wavelength settings on the test light in the bipartite retinal field has been analyzed. Fig. 5 shows the results for a chosen 550 nm wavelength setting and zero net refraction of the tuneable focus lens and negative achromatic lens (i.e., f_1 = 75 mm and f_2 = -75 mm). Evidently, the uncorrected test field translates substantially in the plane of the retina once the pupil entrance point is shifted away from that of the centrally-positioned reference. Thus the predicted test pattern for x = 1.75 and x = 3.50 mm would partially overlap with the reference in the bipartite field (adjacent to the right of the test field shown for x = 0) making a proper determination of relative visibility problematic. The unwanted image translation would commonly have been solved by making mechanical readjustments of the limiting aperture position [1,9].

To confirm the potential of the tuneable focus lens as an alternative for proper refractive correction at a given wavelength the system and eye model was analyzed using different current settings. The unwanted shift of the test field on the retina (as seen in Fig. 5) can be annulled by readjusting the driving current of the tuneable focus lens so that it is brought back to the origin of the bipartite field. This situation is illustrated in Fig. 6 that shows the simulated test pattern without and with proper correction for two off-axis entrance positions of x = 1.75 and x = 3.50 mm for the traversing test beam at 550 nm wavelength. As both the test and the reference light pass the tuneable focus lens, the determined relative visibility in the bipartite field is immune to possible changes in system magnification by the tuning of the lens power.

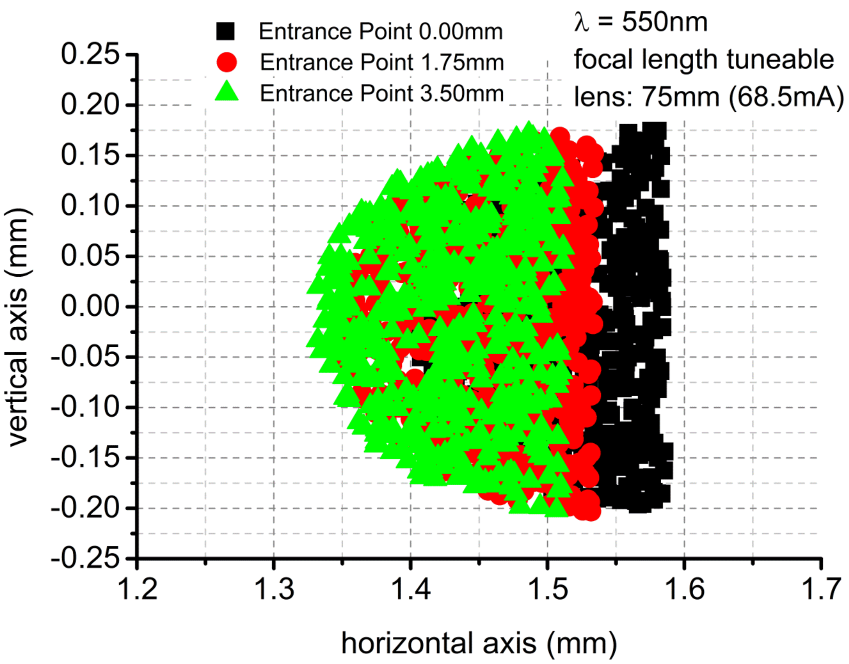

Figure 5. Simulated images of the test pattern in the bipartite retinal field for different positions of the horizontally-traversing beam at the pupil centre (x = 0, black squares), off-axis (x = 1.75 mm, red circles) and near the pupil rim (x = 3.50 mm, green triangles) all for an illumination wavelength of 550 nm. The tuneable focal length is fixed at 75 mm to compensate the power of the -75 mm achromatic lens.

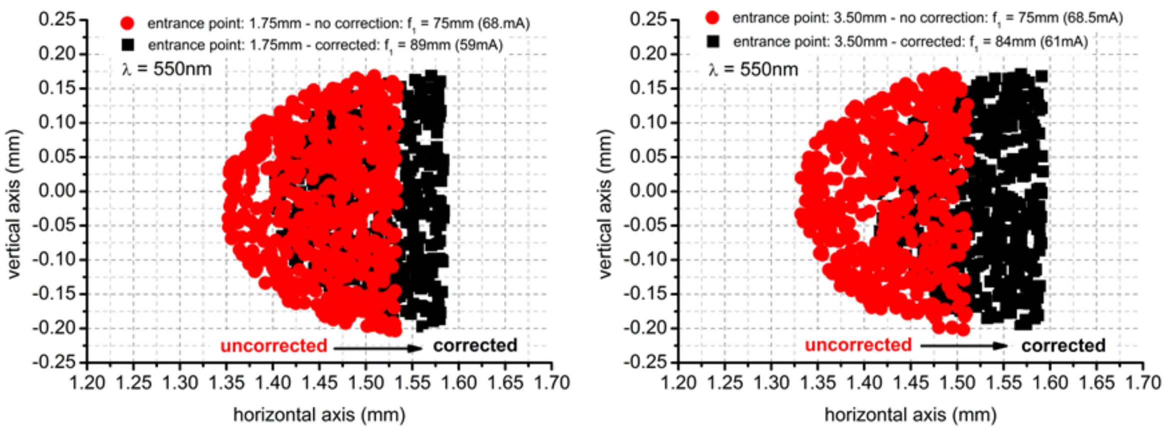

Figure 6. Retinal images of the test in the bipartite field without (red) and with (black) refractive correction using the tuneable focus lens for two off-axis positions: x = 1.75 mm (left) and x = 3.50 mm (right) for an illumination wavelength of 550 nm. The corrective settings correspond to focal lengths of 89 mm and 84 mm for the tuneable focus lens, respectively. After correction the retinal image is identical to the case of x = 0 with f_1 = 75 mm (see Fig. 5).

4. Experimental results and discussion

Three defocus-corrected measurement series (where each series consists of 4 across-the-pupil scans as described in Sec. 2.2) were realized for subjects BV and BL at 11 set wavelengths across the visible spectrum. This large amount of data makes it evident that the automated control of wavelength, brightness, and refractive correction is hugely beneficial to minimize measurement time and fatigue.

4.1 Spectral variations of the Stiles-Crawford visibility function and directionality parameter

For each set wavelength the measured data were fitted to the traditional Stiles-Crawford function given by

$$\eta(x) = 10^{-\rho(x-x_0)^2} \tag{1}$$

where x_0 denotes the pupil asymmetry of the fitting function. In all cases Eq. (1) matched the data with R-squared values of 0.94 or higher determined as the average of three complete measurement series (other fitting functions were also examined but differences were only minor so for simplicity the traditional form of the function was chosen). Relative visibility measurements at 3 distinct wavelength settings are shown in Fig. 7 for both subjects. The error bars indicate the standard deviation for a total of 12 measurements at each pupil point and the solid curve is the best fit based on Eq. (1) using the mean directionality parameter, ρ, determined as the average from the three complete measurement series. As can be noted for subject BL the curve is shifted by 0.3 mm towards the nasal side.

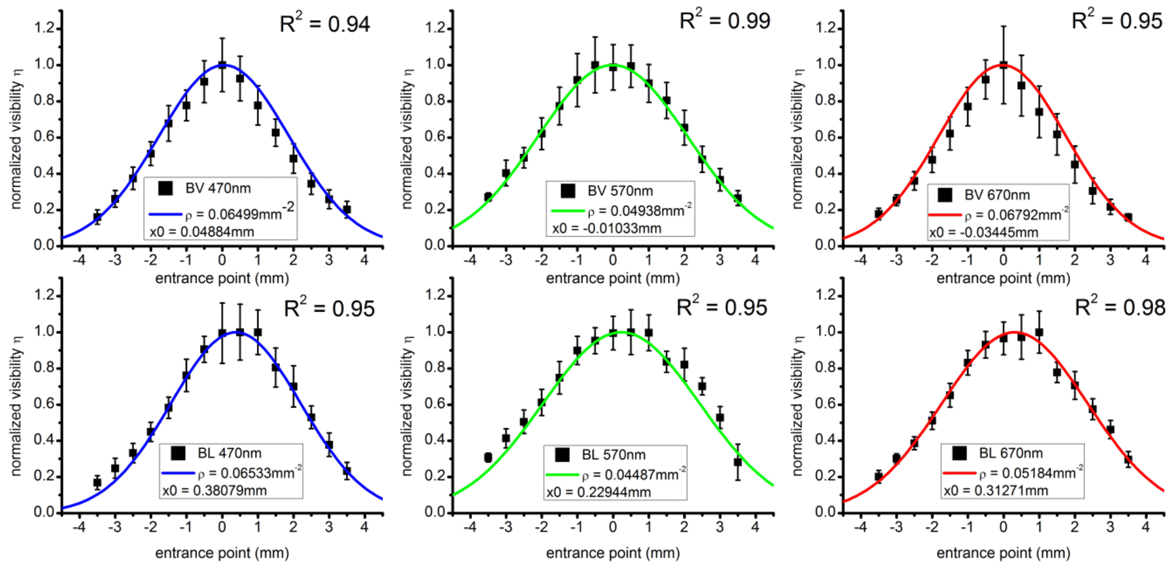

Figure 7. Measured visibility, η, versus pupil point at wavelengths 470, 570 and 670 nm for subjects BV (top) and BL (bottom) obtained after three measurement series (each consisting of 4 across-the-pupil scans). The data (black squares) are shown with standard deviation and the solid coloured line is the best fit for each dataset. The correspondingly-measured directionality parameter, ρ, is indicated in each plot together with the x_0 values.

All the measured data for both subjects have been used to obtain the spectral variation of the visibility parameter the results of which are shown in Fig. 8. For comparison, also data from Stiles' work [9] are shown. As can be seen there is a tendency towards a reduction of the directionality parameter in the green-to-yellow spectral range for both subjects as also observed by Stiles [9] and Enoch [11]. It is worth noting that this coincides approximately with the transition from M to L cones and may therefore relate to the absorption spectra of the individual photopigments or possible waveguide characteristics of the distinct cone types [28]. It implies that the apodization effect of the SCE is less pronounced near the visibility peak of the human eye. Thus, when the directionality is introduced as a pupil apodization in modelling of colour vision it should include the spectral variation of the SCE with strongest apodization in the low and high-wavelength spectral regions.

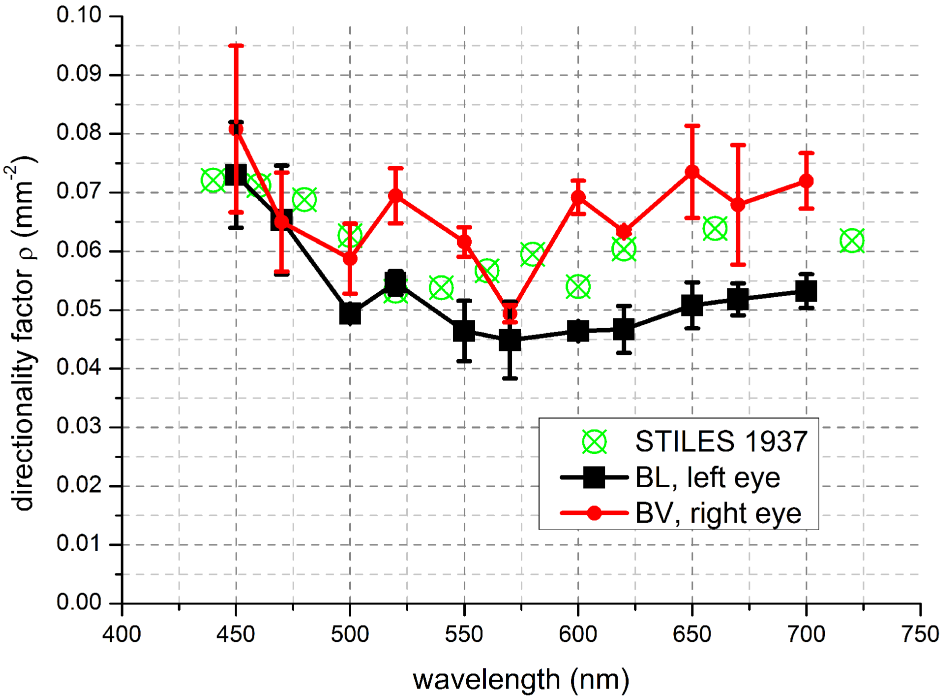

Figure 8. Spectral variation of the directionality factor ρ for both subjects: (BV, red circles) and (BL, black squares) after three complete measurement series (each of which consists of 4 across-the-pupil scans) when determining the visibility at 11 selected wavelengths. In all cases the tuneable focus lens was used for personalized defocus correction in accordance with the calibration shown in Fig. 2. For comparison also data from Stiles' work [9] are shown in the plot (marked with a green ⊗).

4.2 Relation to myopic eyes

Although only two emmetropic subjects have been analyzed it is worth to examine the results in more detail as some insight into the role of eye size and refractive error can be obtained. Fig. 2 has already shown that for the subjects studied a different refractive correction is needed for the unaccommodated eye. Thus one may question the role that myopia might have when determining directionality parameters in SCE characterization.

For a given off-axis pupil point, x, correction of a myopic eye would cause the light to impinge on the retina slightly closer to the photoreceptor axis when compared to an emmetropic or hyperopic case. In consequence an increased visibility should be expected [29]. To get the same angle of incidence on the retina of the uncorrected myopic eye the light ray would have to be shifted further towards the pupil rim by an amount Δx. Thus, comparing the directionality of an emmetropic eye, ρ, to that of a myopic eye, ρ_M, the following relationship should be satisfied: $\rho x^2 = \rho_M (x + \Delta x)^2$. Using geometrical arguments for a simplified eye model where $L_E \sim 17$ mm is the effective axial length of the emmetropic eye (focal length of the relaxed emmetropic eye) and L_M ($>L_E$) is the effective axial length of the myopic eye this can be rewritten as

$$\rho_M = (L_E / L_M)^2 \rho . \qquad (2)$$

The refractive error of the myopic eye increases by approximately 3 dioptres per mm axial length increase [30] and thus Eq. (2) predicts that $\rho_M < \rho_E$. The relation may be rewritten in the following form where D is the number of dioptres of refractive correction

$$\rho_M \approx \left[1 + DL_E\right]^2 \rho . \qquad (3)$$

Take as an example a highly myopic eye with 6 dioptres (D = -6) for which Eq. (3) predicts a directionality parameter of $\rho_M = 0.81\rho$, i.e. a 19% reduction in comparison to that of an emmetropic eye. With a modest 1 dioptre of refractive error the predicted directionality parameter is $\rho_M = 0.97\rho$ or only a 3% drop in comparison to an emmetropic eye. This agrees with reported difficulties in obtaining conclusive evidence of a reduced (or changed) directionality parameter of the myopic eye [13,17]. For highly myopes Choi *et al.* reported a reduction from 0.037/mm^2 (emmetropic) to 0.031/mm^2 (highly myopic) for the foveal region which corresponds to a ratio of 0.84 in good agreement with the estimates above. However, one cannot exclude the possibility of a minor reorientation of cones in highly myopic or hyperopic eyes that may also impact the measurements although cones are known to be well aligned towards the centre of the entrance pupil [31]. Eq. (3) also predicts that hyperopes ($D > 0$) would tend to have a higher directionality than emmetropes although, with the exception of one eye [13], this has to our knowledge not been examined in any detail yet.

For the two subjects considered in this study the refractive difference is only minor. Their spherical equivalent differs by 0.38D implying that subject BL would have a slightly lower directionality parameter than subject BV. The difference based on Eq. (3) is only about 1% which is less than seen in Fig. 8. Given the large uncertainty in the directionality measurements, however, more subjects would still need to be analyzed to narrow down the possible reasons for the subjective differences in the SCE results.

5. Conclusions

A tuneable focus lens has been implemented and analyzed in a bipartite SCE characterization system and narrowband visibility measurements have been realized in two subjects across the visible spectrum to determine the spectral variation of the characteristic directionality parameter. The lens corrects subjective refractive error and also minor remnant system aberrations. The results of directionality show good correspondence to the majority of previous measurements at selected wavelengths and across the visible spectrum although for the latter available data in the literature is still rather limited. The tuneable focus lens has the advantage of requiring no external mechanical adjustments and thus it allows for a more automated analysis of the SCE than with previous systems that all required mechanical readjustments when the wavelength being tested was changed.

The smallness of light beams when entering the eye makes it unlikely that higher-order aberrations impact the directionality measurements in the setup although they do play a role for large pupils and an integrated SCE [5] although less so under normal visual conditions [32]. The tuneable focus lens is a first step towards implementing adaptive optics for SCE analysis to more accurately control the light impinging on the retina. This would have improved potential for analysing the role of wavefront phase directly at the retina at the level of individual cones [33]. A detailed understanding of the light to photoreceptor coupling across the visible spectrum is essential to unlock the remaining secrets of how an image is optically coupled to the photoreceptor pigments as the last optical step prior to neural responses [5].

Acknowledgments

The authors wish to thank J. A. Diaz (Universidad de Granada, Spain) for providing Zemax eye model files and his detailed support. Also, the help of R. McQuaid and A. Cummings (Wellington Eye Clinic, Ireland) in determining the axial length and refractive error of the author's eyes is gratefully acknowledged. This research has been realized with financial support from Science Foundation Ireland (grants: 07/SK/B1239a and 08/IN.1/B2053), the Irish Research Council and Alcon Laboratories Inc.

References

[1] Stiles W S and Crawford B H 1933 The luminous efficiency of rays entering the eye pupil at different points *Proc. Roy. Soc. B* **112** 428-450

[2] Westheimer G 2008 Directional sensitivity of the retina: 75 years of Stiles-Crawford effect *Proc. Roy. Soc. B* **275** 2777-2786

[3] Enoch J M 1963 Optical properties of the retinal receptors *J. Opt. Soc. Am.* **53** 71-85

[4] Matsumoto C S, Shinoda K, Matsumoto H, Satofuka S, Mizota A, Nakatsuka K and Miyake Y 2012 Stiles-Crawford effect in focal macular ERGs from macaque monkey *J. Vision* **12** art. 6.

[5] Vohnsen B 2007 Photoreceptor waveguides and effective retinal image quality *J. Opt. Soc. Am. A* **24** 597-607

[6] Hárosi F I and Flamarique I N 2012 Functional significance of the taper of vertebrate cone photoreceptors *Gen. Physiol*. **139** 159–187

[7] Westheimer G 2013 Retinal light distributions, the Stiles–Crawford effect and apodization *J. Opt. Soc. Am. A* **30** 1417-1421

[8] Westheimer G, 1966 The Maxwellian view *Vision Res*. **6** 669-682

[9] Stiles W S 1937 The luminous efficiency of monochromatic rays entering the eye pupil at different points and a new colour effect *Proc. Roy. Soc. B* **123** 90-118

[10] Enoch J M and Stiles W S The colour change of monochromatic light with retinal angle of incidence *Optica Acta* **8** 329-358

[11] Enoch J M 1958 Summated response of the retina to light entering different parts of the pupil *J. Opt. Soc. Am.* **48** 392-405

[12] Kruger P B, Lopez-Gil N and Stark L R 2001 Accommodation and the Stiles-Crawford effect: theory and a case study *Opthal. Physiol. Opt.* **21** 339-351

[13] Choi S S, Garner L F and Enoch J M 2003 The relationship between the Stiles-Crawford effect of the first kind (SCE-I) and myopia *Ophthal. Physiol. Opt.* **23** 465-472

[14] Lochocki B, Rativa D and Vohnsen B 2011 Spatial and spectral characterisation of the first and second Stiles-Crawford effects using tuneable liquid-crystal filters *J. Mod. Opt.* **58** 1817-1825

[15] Rativa D and Vohnsen B 2011 Single- and multimode characteristics of the foveal cones: the super-Gaussian function *J. Mod. Opt.* **56** 1809-1816

[16] Alpern M and Kitahara K 1983 The directional sensitivities of the Stiles' colour mechanisms *J. Physiol.* **338** 627-649

[17] Singh N, Atchison D A, Kasthurirangan S and Guo H 2009 Influences of accommodation and myopia on the foveal Stiles-Crawford effect *J. Mod. Opt*. **56** 2217-2230

[18] Nordby K and Sharpe L T 1988 The directional sensitivity of the photoreceptors in the human achromat *J. Physiol.* **399** 267-281

[19] Enoch J M and Hope G M 1973 Directional sensitivity of the foveal and parafoveal retina. *Inv. Opthalmol.* **12** 497-503

[20] Applegate R A and Lakshminarayanan V 1993 Parametric representation of Stiles-Crawford functions: normal variation of peak location and directionality *J. Opt. Soc. Am. A* **10** 1611-1623

[21] Fincham E F 1951 The accommodation reflex and its stimulus *Br. J. Opthalmol.* **35** 381-393

[22] Enoch J M and Lakshminarayanan V 2009 Integration of the Stiles-Crawford effect of the first kind *J. Mod. Opt.* **56** 2240-2250

[23] Vohnsen B and Rativa D 2011 Absence of an integrated Stiles-Crawford function for coherent light *J. Vision* **11** 1-10

[24] Bedford R E and Wyszecki G 1957 Axial chromatic aberration of the human eye *J. Opt. Soc. Am.* **37** 564-565

[25] Crawford B H 1937 The luminous efficiency of light entering the eye pupil at different points and its relation to brightness threshold measurements, *Proc. Roy. Soc. B* **124** 81-96

[26] http://www.optotune.com/index.php?option=com_content&task=view&id=18&Itemid=37. Access Date: 23.05.2013

[27] Diaz J A, Pizarro C and Arasa J 2008 Single dispersive gradient-index profile for the aging human lens *J. Opt. Soc. Am. A* **25** 250-261

[28] Vohnsen B 2009 On the spectral relation between the first and second Stiles-Crawford effect *J. Mod. Opt.* **56** 2261-2271

[29] Snyder A W and Pask C 1973 The Stiles-Crawford effect – explanation and consequences *Vision Research* **13** 1115-1136

[30] Lens A, Nemeth S C and Ledford J K 2008 “Ocular anatomy and physiology” (Slack Inc. 2008) p. 158.

[31] Laties A M and Enoch J M 1971 An analysis of retinal receptor orientation *Invest. Ophthalmol.* **10** 69-77

[32] Atchison D A, Joblin A and Smith G 1998 Influence of Stiles-Crawford effect apodization on spatial visual performance *J. Opt. Soc. Am. A* **15** 2545-2551

[33] Harmening W M, Tiruveedhula P, Roorda A, and Sincich L C 2012 Measurement and correction of transverse chromatic offsets for multi-wavelength retinal microscopy in the living eye *Biomed. Opt. Express* **3** 2066-2077